Electrocatalytic Formate Oxidation by Cobalt-Phosphine Complexes

Sriram Katipamula, Andrew W. Cook, Isabella Niedzwiecki, Thomas J. Emge, Kate M. Waldie*

Department of Chemistry and Chemical Biology, Rutgers, The State University of New Jersey, Piscataway, New Jersey 08854, United States

*kate.waldie@rutgers.edu

ABSTRACT

We report a family of cobalt complexes based on bidentate phosphine ligands with two, one, or zero pendent amine groups in the ligand backbone. The pendent amine complexes are active electrocatalysts for the formate oxidation reaction, generating CO_2 with near-quantitative faradaic efficiency at moderate overpotentials (0.45 – 0.57 V in acetonitrile). These homogeneous electrocatalysts are the first cobalt example and second first-row transition metal example for formate oxidation. Thermodynamic measurements reveal these complexes are energetically primed for formate oxidation via hydride transfer to the cobalt center, followed by deprotonation of the resulting cobalt-hydride by formate acting as a base. The complex with the strongest cobalt-hydride bond, given by its thermodynamic hydricity, is the fastest electrocatalyst in this series, with an observed rate constant for formate oxidation of 135 ± 8 h^{-1} at 25 °C. Electrocatalytic turnover is not observed for the complex with no pendent amine groups: decomposition of the complex structure is evident in the presence of high formate concentrations.

INTRODUCTION

The large-scale implementation of renewable energy technologies continues to drive interest in using chemical fuels as energy carriers to bridge the gap between intermittent electricity availability and global demand. Within this scheme, the shift toward fuel cells to replace traditional fossil fuel combustion is attractive for the extraction of usable energy from chemical fuels. While H_2 has drawn considerable interest as an energy carrier to mitigate our reliance on fossil resources and enable our renewable energy future,[1-4] the challenges associated with safe storage and transportation of H_2 gas have hindered the realization of a hydrogen economy.[5] Formic acid

represents an appealing alternative to H_2, offering distinct advantages in terms of safety, storage, and handling thanks to its liquid state, chemical stability, low ignition point, and low toxicity.[6-7] Thus, the development of electrocatalysts to mediate the $2e^-$,$1H^+$ oxidation of formate is an active research area to advance formic acid as an energy carrier (Figure 1a).[8]

Heterogeneous electrocatalysts for formate oxidation are largely based on noble metal systems.[8-13] To the best of our knowledge, only three examples of homogeneous electrocatalysts for formate oxidation have been reported to date (Figure 1b).[14-17] Kubiak and co-workers disclosed the first example utilizing a series of nickel P_2N_2 complexes as electrocatalysts, where P_2N_2 = 1,5-diaza-3,7-diphosphacyclooctane.[14-15] The pendent amines in the P_2N_2 ligand were shown to be critical for electrocatalytic turnover: the nickel depe analogue was not active for formate oxidation (depe = 1,2-bis(diethylphosphino(ethane)). While the precise mechanism of formate oxidation remains in question,[15, 18] direct hydride transfer from formate to the Ni^{II} center to generate a Ni^{II}-hydride intermediate may be operative. Later work by Kang and co-workers achieved bi-directional formate oxidation-CO_2 reduction using an iridium pincer electrocatalyst.[16] Yang and co-workers developed a reversible electrocatalytic system for formate-oxidation-CO_2 reduction based on a platinum diphosphine complex.[17] For the two noble metal systems, formate oxidation is proposed to occur through hydride transfer.

The favorability of hydride transfer reactions can be readily quantified using thermodynamic hydricity.[19] The hydricity of the formate anion in acetonitrile is 44 kcal/mol.[20] To promote heterolytic cleavage of the formate C-H bond via hydride transfer to a metal center, the hydricity of the resulting metal-hydride bond must be greater than this value. We[21] and others[22-23] have previously reported $CpCo^{III}$(diphosphine)-hydride complexes (Cp = cyclopentadienyl ligand) to have hydricities near 70 kcal/mol. Thus, this architecture should be poised for energetically favorable formate oxidation. While select $CpCo^{II}$-hydrides have been exploited for electrocatalytic reduction reactions including H_2 evolution and CO_2 reduction,[23-26] Co^{III}-hydrides have not been explored within the context of electrocatalysis.

The anticipated thermodynamic driving force for hydride transfer from formate to the Co^{III} center led us to prepare a series of $[CpCo^{III}(P\text{-}P)(MeCN)]^{2+}$ complexes **1**-**3** for investigation (Figure 1c). Given the importance of the pendent amines for achieving formate oxidation at the nickel P_2N_2 systems[14] and the proposed roles of this ligand class for facilitating intramolecular proton transfer and transition state stabilization in several other catalytic systems,[26-34] we targeted complexes

containing the P_2N_2 ligand as well as the related PNP and dppp ligands, which have one and zero pendent amine groups, respectively, to probe the influence of the amine functionality on activity. Herein, we report our investigations into this family of cobalt complexes and show that **1** and **2** are active electrocatalysts for the selective oxidation of formate to CO_2 at ambient conditions. The thermodynamic properties of these complexes are reported, which confirm the large hydride affinity of **1**-**3**. The electrocatalytic activity for formate oxidation is quantified by chronoamperometry and controlled-potential electrolysis, revealing **2** as the best performing electrocatalyst in this series.

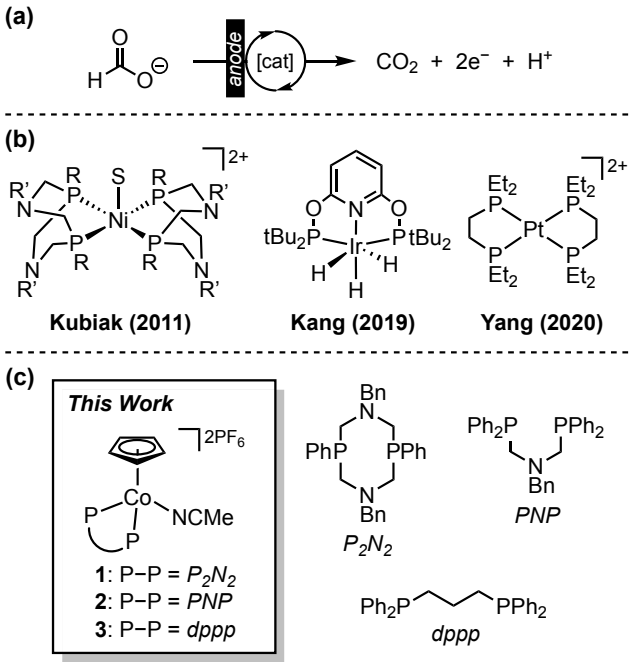

Figure 1. (a) Previous examples of molecular electrocatalysts for formate oxidation.[14-17, 35-36] (b) Cobalt complexes **1-3** from this work.

RESULTS AND DISCUSSION

Synthesis and Characterization. The PNP and P_2N_2 ligands were synthesized following literature procedures.[37-38] Complexes **1**-**3** were prepared by the reaction of the desired phosphine ligand with [CpCo(CO)I_2], followed by halide abstraction using $AgPF_6$ (2.2 eq) (Scheme 1).[39] Each complex was isolated as a red crystalline solid in reasonable yield following recrystallization from diethyl ether/acetonitrile. These complexes are air and moisture stable in solution over several

days. The ^{1}H NMR spectra of **1**-**3** show a sharp singlet at 5.5–5.7 ppm corresponding to the Cp ligand. The ^{31}P NMR spectra display one singlet for the phosphine ligand near 30 ppm. These values are typical of CpCo^{III}-phosphine complexes and indicate that the pendent amine groups do not substantially influence the NMR characteristics of these systems.[21, 26, 40-41]

Scheme 1. Synthesis of complexes **1**-**9**.

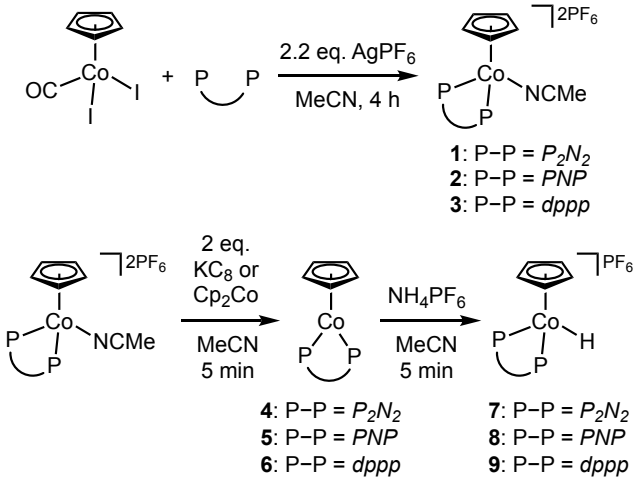

The synthesis of the Co^{I} (**4**-**6**) and Co^{III}-hydride (**7**-**9**) complexes was adapted from literature procedures for related systems (Scheme 1).[23] In brief, complexes **1**-**3** were treated with 2 eq chemical reductant (KC_8 or cobaltocene) to obtain **4**-**6** as dark red solids, and subsequent protonation with 1 eq NH_4PF_6 yielded Co^{III}-hydrides **7**-**9** as bright yellow crystalline powders. We note that while **7**-**9** are highly air-sensitive, they remain stable in acetonitrile under N_2 for several days. By ^{1}H NMR, the Cp signals of **4**-**6** are observed at 4.4-4.5 ppm, shifted upfield by more than 1 ppm compared to the respective signals in **1**-**3**. These chemical shift changes are consistent with a decrease in metal oxidation state and complex charge upon reduction from [Co^{III}-MeCN]$^{2+}$ to [Co^{I}]^{0}. The signal is shifted downfield to ca. 4.8 ppm for Co^{III}-hydride **7**-**9**, as expected for protonation of [Co^{I}]^{0} to [Co^{III}-H]$^{+}$.[40-41] The diagnostic ^{1}H NMR hydride signal for **7-9** appears as a well-resolved triplet at ca. -14 ppm. As with **1**-**3**, the phosphorus ligand identity has minimal effect on the NMR spectra for this series.

Crystals suitable for X-Ray crystallography were obtained via vapor diffusion of diethyl ether into acetonitrile (for **3**, **7**, and **9**) or dichloromethane (for **2**), or by slow cooling of a concentrated solution in acetonitrile (for **4** and **5**), tetrahydrofuran/diethyl ether (for **6**), or acetonitrile/diethyl

ether (for **8**). The structures of the PNP complexes are highlighted in Figure 2. All other structures, along with selected bond lengths and angles, are provided in the Supporting Information. The crystal structure of **1** was previously reported by Artero and co-workers.[26] As expected, all Co^{III} complexes adopt a three-legged piano-stool geometry based on the planar η^5-Cp ligand and bidentate phosphine ligand. The final coordination site is occupied by either acetonitrile (**1**-**3**) or a hydride ligand (**7**-**9**). The PNP and dppp ligands both form a six-membered metallocycle in a chair conformation with the Co^{III} center, while the P_2N_2 in **7** forms two six-membered rings analogous to **1**: one in a chair conformation, one in a boat conformation. The structures of **4**-**6** exhibit a two-legged piano-stool geometry, which is typical of half-sandwich Co^{I} complexes.[21] The η^5-Cp ligand and the P1–Co–P2 plane are approximately perpendicular. There is a general increase in the Co–P bond lengths within each compound class following P_2N_2 < PNP < dppp. This trend is consistent with the greater electron donating character of the P_2N_2 ligand in which each phosphine has one phenyl and two alkyl groups, as opposed to the one alkyl and two phenyl groups in the PNP and dppp ligands.

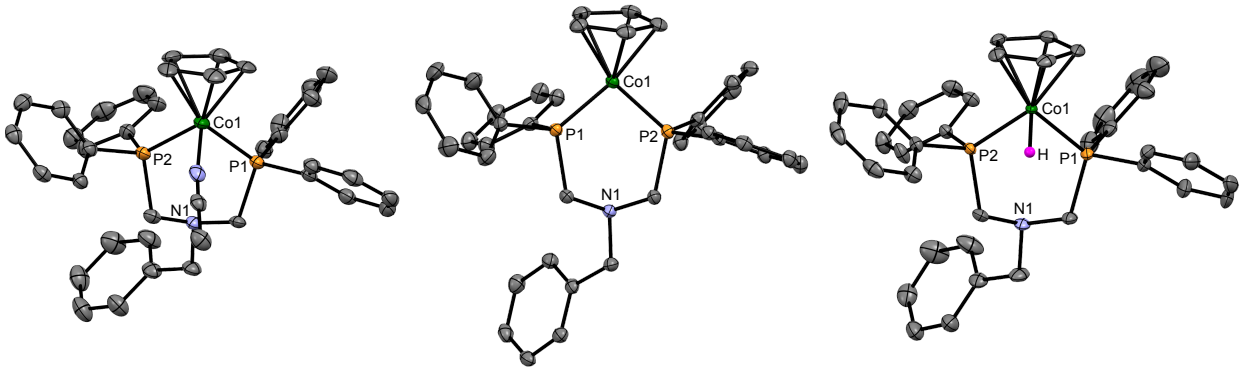

Figure 2. Structures of PNP complexes **2** (left), **5** (center), and **8** (right). Hydrogen atoms, co-crystallized solvent molecules, and PF_6^- counterions omitted for clarity. Ellipsoids shown at 50% probability.

Electrochemical Studies. Cyclic voltammetry (CV) was used to probe the electrochemical behavior of **1**-**3** in 0.1 M [^{n}Bu$_4$N][PF$_6$] in acetonitrile. Each complex displays two reversible one-electron reductions (Figure 3 and Table 1), which are assigned to the $Co^{III/II}$ and $Co^{II/I}$ couples, respectively.[19, 21, 24, 26, 40-41] In all cases, the peak currents vary linearly with the square root of the scan rate ($v^{1/2}$), indicating diffusion-controlled electron transfer (Figures S37-S42). Complexes **2**

and **3** exhibit very similar potentials for both redox processes (within 50 mV), while the reduction potentials for **1** are ca. 200 mV more negative. As noted above, this trend is consistent with the greater electron donating character of the P_2N_2 ligand.

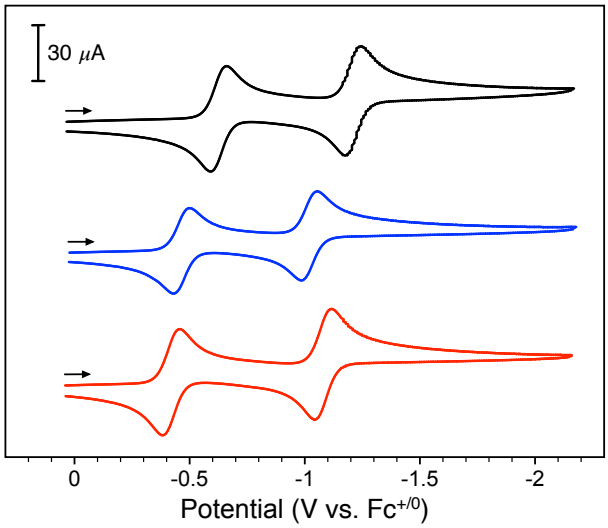

Figure 3. CVs of **1** (black trace), **2** (blue trace) and **3** (red trace) in acetonitrile. Scan rate = 100 mV/s.

Table 1. CV data for Complexes **1**-**3**.[a]

complex	$E_{1/2}$ (V)[c]	ΔE_p (mV)[d]	i_c/i_a[e]	$E_{1/2}$ (V)[c]	ΔE_p (mV)[d]	i_c/i_a[e]
1	-0.64	84	1.03	-1.21	91	1.01
2	-0.47	68	0.98	-1.02	63	1.01
3	-0.42	72	1.05	-1.07	66	1.06
1[b]	-0.95	106	1.08	-1.21	72	1.01
2[b]	-0.83	76	1.05	-1.02	68	1.00
3[b]	-0.75	70	1.02	-1.08	67	1.01

[a]1 mM [Co] in 0.1 M [^{n}Bu$_4$N][PF$_6$] in acetonitrile, glassy carbon working electrode, Pt wire counter electrode, Ag/AgNO$_3$ reference electrode. 100 mV/s. [b]With 10 mM [^{n}Bu$_4$N][(HCO$_2$)$_2$H]. [c]$E_{1/2}$ = (E_{pa} + E_{pc})/2, where E_{pa} and E_{pc} are anodic and cathodic peak potentials, respectively. Potentials in V vs. Fc$^{+/0}$. [d]$\Delta E_p = E_{pa} - E_{pc}$. [d]$i_c$ = cathodic peak current, i_a = anodic peak current.

Thermodynamic Properties. Given the relevance of thermodynamic hydricity (ΔG_{H-}) to the oxidation of formate, we sought to experimentally determine this value for Co^{III}-hydrides **7**-**9**. There are three well-established methods for measuring the hydricity of metal-hydride complexes: here, we use the *potential-pK_a* approach outlined in Scheme 2.[19] In this thermochemical cycle, the free energy associated with the $Co^{III/II}$ and $Co^{II/I}$ redox couples and the acidity of the Co^{III}-hydride are combined with the free energy for two-electron reduction of a proton to a hydride to obtain the thermodynamic hydricity according to equation 6.[42] As noted with other systems, this value could be considered an *effective hydricity* measurement since coordination of an acetonitrile ligand to the Co^{III} center occurs following hydride loss from the Co^{III}-hydride, and thus the free energy associated with this coordination event is implicitly included in this calculation.[43]

Scheme 2. Potential-pK_a method for determining the hydricity of Co^{III}-hydrides **7**-**9**. S = acetonitrile. Reaction free energies in kcal/mol.

$$[L_nCo^{III}\text{–}H]^+ \rightleftharpoons [L_nCo^{I}] + H^+ \qquad 1.364\ pK_a \qquad (1)$$

$$[L_nCo^{I}] \rightleftharpoons [L_nCo^{II}]^+ + e^- \qquad 23.06\ E_1^\circ \qquad (2)$$

$$[L_nCo^{II}\text{–}S]^+ \rightleftharpoons [L_nCo^{III}\text{–}S]^{2+} + e^- \qquad 23.06\ E_2^\circ \qquad (3)$$

$$H^+ + 2\,e^- \rightleftharpoons H^- \qquad 79.6 \qquad (4)$$

$$[L_nCo^{III}\text{–}H]^+ \overset{S}{\rightleftharpoons} [L_nCo^{III}\text{–}S]^{2+} + H^- \qquad \Delta G^\circ_{H-} \qquad (5)$$

$$\Delta G^\circ_{H-} = 1.364\ pK_a + 23.06\ E_1^\circ + 23.06\ E_2^\circ + 79.6 \qquad (6)$$

The relevant redox potentials for **1**-**3** were measured by CV (*vide supra*). The pK_a of Co^{III}-hydride **7**-**9** was measured by UV-vis spectrophotometric titration in acetonitrile/toluene (90:10) to solubilize both the Co^{III}-hydride and Co^{I} complexes.[40-41] Addition of an appropriate base, either triethylamine (pK_a = 18.4)[44] or DBU (1,8-diazabicyclo[5.4.0]undec-7-ene, pK_a = 24.3)[44], to a 0.55 mM solution of Co^{III}-hydride **7**-**9** leads to formation of the conjugate base **4**-**6**, respectively (Figures S57-S59). From these data, the pK_a of **8** and **9** are calculated to be identical within experimental error (pK_a = 19.8), while the pK_a of **7** is 23.1 (Table 2), in line with the greater electron donating character of the P_2N_2 ligand (*vide supra*). The initial and final absorbance spectra in these titrations match the UV-vis spectra of independently prepared solutions of each Co-hydride and Co^{I} complex. The spectra of the Co-hydride complexes show a main absorption at ca. 360 nm, and the Co^{I} species show absorption features at ca. 380 and 480 nm (Figures S45-S56).

Using equation 6 with the experimental redox and pK_a data, we obtain the thermodynamic hydricity of each Co^{III}-hydride (Table 2). The P_2N_2 complex **7** is the strongest hydride donor in this series, with ΔG_{H-} = 68.5 kcal/mol. The PNP and dppp complexes (**8** and **9**, respectively) both have hydricity values of 72.3 kcal/mol, making these species slightly poorer hydride donors compared to **7**. Previous reports have demonstrated linear correlations between thermodynamic hydricity and the first reduction potential of the parent complex, and pK_a and the second reduction of the parent complex for several nickel,[19] palladium,[45] and other[22,46] hydrides. As expected, these cobalt systems display similar linear trends (Figures S60-S61). We note that hydride affinity is given by the reverse reaction of hydricity (i.e., hydride affinity = $-\Delta G_{H-}$): thus, the P_2N_2 complex **1** is the weakest hydride acceptor in this series, while PNP and dppp complexes (**2** and **3**, respectively) have similar hydride affinities.

Table 2. Summary of electrochemical and thermodynamic data in acetonitrile.

ligand	$E_{1/2}[Co^{III/II}]$ [a]	$E_{1/2}[Co^{II/I}]$ [a]	pK_a of Co^{III}-H	ΔG_{H-} of Co^{III}-H [b]
P_2N_2	-0.64	-1.21	23.1	68.5
PNP	-0.47	-1.02	19.8	72.3
dppp	-0.42	-1.07	19.8	72.3

[a]Potentials in V vs. $Fc^{+/0}$. [b]Hydricity (ΔG_{H-}) in kcal/mol.

Chemical Reactivity Studies with Formate. The hydricity of formate in acetonitrile is 44 kcal/mol.[20] Given the experimentally determined hydricity values for **7**-**9** (Table 2), the hydride affinity of each Co^{III}-acetonitrile complex is such that hydride transfer from formate to the metal center is predicted to be highly thermodynamically favorable. We first sought to investigate the chemical reactivity of **1**-**3** with formate under pseudo-first order conditions. Treatment of **1** or **2** with 15 eq formate (added as the soluble biformate salt [^{n}Bu$_4$N][(HCO$_2$)H])[14] in CD_3CN results in the generation of the corresponding Co^I species **4** or **5** based on ^{1}H NMR (Figure S71-S72). We repeated this experiment on a larger scale in a gastight flask and sampled the reaction headspace by gas chromatography. Quantitative formation of CO_2 (relative to cobalt) was observed after 150 s, confirming stoichiometric formate oxidation (Scheme 3 and Table S11). This reactivity is

consistent with hydride transfer from formate to generate a Co^{III}-hydride, followed by proton transfer where formate acts as a base (the estimated pK_a of formic acid in acetonitrile is 20.9).[47] Indeed, in separate experiments, we find that treatment of the Co^{III}-hydrides with 10 eq formate results in rapid formation of the Co^{I} complexes. The addition of formate to **3** also results in stoichiometric formate oxidation; however, the yield of CO_2 is lower (63 ± 5%) and free dppp ligand is observed by ^{31}P NMR (Figure S74), indicating partial decomposition of the cobalt complex. Thus, these experiments indicate that **1** and **2** are capable of key chemical steps leading to formate oxidation and are viable electrocatalyst candidates, while **3** shows limited stability in the presence of high formate concentrations.

Scheme 3. Proposed stepwise reactivity of **2** with 15 eq formate.

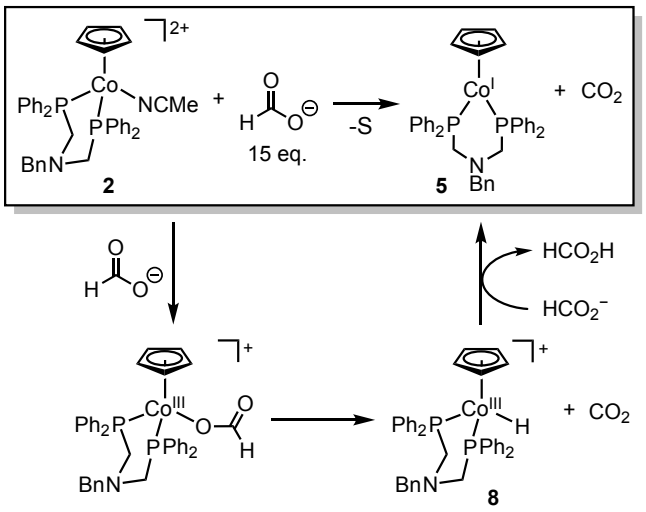

We also examined the stoichiometric behavior of **1**-**3** with formate by ^{1}H NMR. Upon addition of 1 eq formate to **3** in CD_3CN, a new species is immediately formed, assigned as the Co^{III}-formate adduct (Figure S75). Resonances associated with a paramagnetic species are also observed, which gradually increase in intensity over time as the Co^{III}-formate signals decrease. The paramagnetic species is assigned as $[CpCo^{II}(dppp)]^+$ based on comparison to an independently prepared sample obtained via chemical reduction of **3** with 1 eq cobaltocene (Figure S76). After 1 h, signals for Co^{III}-hydride **9** appear and continue to grow, reaching ca. 50 % yield after 10 h (Figure S77-S78). Complexes **1** and **2** show comparable behavior with equimolar formate (Figure S80-S82). We recently reported similar reactivity of a related [CpCo] complex at 65 ºC, which we

attributed to slow hydride transfer from formate, followed by rapid equilibria for the deprotonation of the Co^{III}-hydride and the comproportionation of the resulting Co^{I} with Co^{III}-X (X = MeCN or formate).[21] Here, we propose the analogous reactivity is operative with **1**-**3** with 1 eq formate at 25 ºC (Figure S79). Note, no significant decomposition of **3** is observed under these conditions.

In this scheme, the favorability of the comproportionation reaction of Co^{I} with Co^{III}-X (X = MeCN or formate) is easily obtained from the difference in $Co^{III/II}$ and $Co^{II/I}$ redox potentials (Table S12). We also observe that the protonation of **4**-**6** with formic acid is facile and rapid – the protonation rate constant is measured to be on the order of 10^6 M^{-1} s^{-1} using established CV methods (see Supporting Information).[48] Additionally, attempts to isolate single crystals of $[CpCo(dppp)(formate)]^+$ instead yielded crystals of $[CpCo^{II}(dppp)]^+$ (Figure S9), further supporting the presence of this species in the reaction solution.

Electrocatalytic Formate Oxidation. Our chemical reactivity studies clearly indicate that **1** and **2** can mediate stoichiometric formate oxidation to generate CO_2 in quantitative yield. Thus, we also investigated their activity for the electrocatalytic oxidation of formate by electrochemical methods. Upon addition of 10 eq formate to the CV solution of **1**-**3**, the open-circuit potential of the electrochemical cell changes dramatically (Figure 4a and S43-S44), shifting from ca. 0 V vs. $Fc^{+/0}$ (more positive than the $Co^{III/II}$ redox couple) in the absence of formate to ca. -1.5 V vs. $Fc^{+/0}$ (more negative than the $Co^{II/I}$ redox couple) with formate added to the solution. This behavior is indicative of a significant change in the composition of the bulk solution, and is consistent with the formation of Co^{I} according to Scheme 3. Electrochemical oxidation of the Co^{I} complex occurs at the electrode as the potential is swept in the positive direction; however, the CV data shows no appreciable enhancement in peak currents, indicating that electrocatalytic turnover is not observable on this timescale.

The CV studies of **1**-**3** in the presence of formate also reveal a significant shift (ca. 300 mV) in the $Co^{III/II}$ redox couples to more negative potentials (Figure 4a and S43-S44). Previous work by Dempsey and co-workers showed that $[CpCo(P–P)(MeCN)]^{2+}$ complexes undergo one-electron reduction by an *EC* mechanism where reversible loss of the acetonitrile ligand occurs at the Co^{II} state.[40-41] Given this precedent, an *EC* mechanism involving formate is reasonable for the first reduction process, where the reversible binding of formate occurs at the intermediate Co^{II} species. Since formate is an anionic ligand, the Co^{III}-formate/Co^{II}-formate couple occurs at a more

negative potential compared to that of the Co^{III}-acetonitrile complex. The $Co^{II/I}$ redox couple is unaffected by the presence of formate in solution (Table 1).

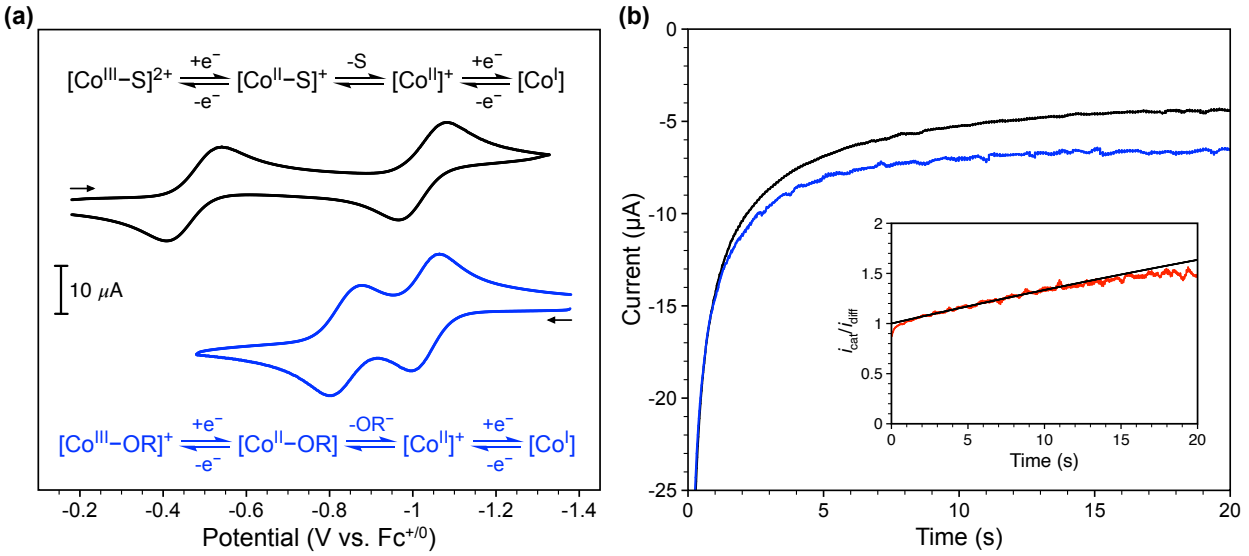

Figure 4. (a) Cyclic voltammograms and proposed reactivity pathways for **2** (0.5 mM, black) and **2** with 10 eq formate (blue) in acetonitrile. S = acetonitrile. OR^- = formate. Scan rate = 100 mV/s. (b) Chronoamperometry of **5** (0.5 mM, black trace) and **5** with 50 eq formate (blue trace) in acetonitrile at η = 200 mV (E_{app} = -0.27 and -0.63 V vs. $Fc^{+/0}$, respectively). Inset: Current ratio of the chronoamperometry traces (red trace) and fit between 5 and 10 s (black trace).

Since no electrocatalytic currents were observed by CV, we turned to chronoamperometry (CA) to further probe the reactivity of **1** and **2** with formate. CA methods can be utilized to extract an observed rate constant (k_{obs}) for electrocatalytic reactions, and this approach can be especially useful for reactions where $k_{obs} < 1\ s^{-1}$.[48-49] For our CA studies, we started with Co^I complex **4** or **5** (0.5 mM) in 0.1 [^{n}Bu$_4$N][PF$_6$] in acetonitrile such that an oxidative potential step could be applied to the system. Formate (50 eq) was then added to the solution and the CA experiment was repeated. In each case, the applied potential was held 200 mV more positive than the appropriate $Co^{III/II}$ oxidation potential: Co^{III}-MeCN/Co^{II}-MeCN or Co^{III}-formate/Co^{II}-formate for 0 or 50 eq formate, respectively. As shown in Figure 4b, a current enhancement is achieved with **5** in the presence of formate, indicating electrocatalysis (Figure 4b). The ratio of these two CA traces was fit to the equation describing an *EC'* mechanism (see Supporting Information), from which k_{obs} is estimated

to be 135 ± 8 h^{-1}. With complex **4**, these CA traces are identical within experimental error (Figure S62), indicating that any electrocatalysis is too slow to quantify by this technique; we estimate the upper limit for electrocatalytic formate oxidation to be 4 h^{-1}.

To confirm that electrocatalytic formate oxidation is operative with **1** and **2**, we further examined the electrocatalytic behavior by controlled-potential electrolysis (CPE). In these studies, the working electrode potential was held ca. 150 mV more positive than the Co^{III}-formate/Co^{II}-formate oxidation potential to ensure rapid electron transfer. Using **1** or **2** in the presence of 50 eq formate, a stable current was obtained over 95 min, with **2** consistently achieving higher current densities (Figure 5). Analysis of the headspace by gas chromatography confirms CO_2 production with high faradaic efficiency over multiple turnovers (Table 3). Additionally, no CO production is observed. CVs of the solution recorded after electrolysis still show the $Co^{III/II}$ and $Co^{II/I}$ redox couples associated with **1** and **2**: ca. 75% of the catalyst remains intact based on the peak current of the $Co^{II/I}$ oxidation wave recorded before and after CPE (Figures S64-S67). The analogous CPE control experiments in the absence of cobalt catalyst show low current densities and negligible charge passed (Figure 5).

Controlled-potential electrolysis with **3** under the same conditions did not result in productive electrocatalysis. Minimal current densities were achieved with this system, and CVs recorded after electrolysis show no identifiable redox features. These results further confirm the decomposition of **3** with high levels of formate. The reasons for the limited stability of this complex in comparison to **1** and **2** are unclear. The decomposition of cobalt complexes under electrochemical conditions has been noted in select cases.[50-54]

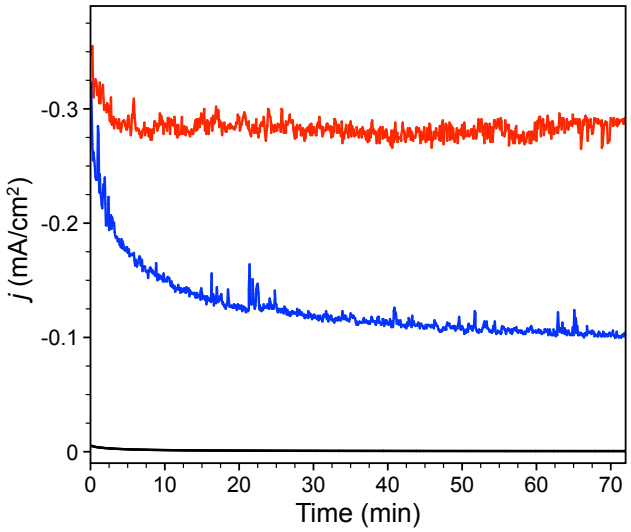

Figure 5. CPE current density traces for formate oxidation with **1** (0.35 mM, E_{app} = -0.80 V vs. $Fc^{+/0}$, blue trace) or **2** (0.35 mM, E_{app} = -0.68 V vs. $Fc^{+/0}$, red trace) with 50 eq formate in acetonitrile. Control experiment in the absence of cobalt at E_{app} = -0.65 V vs. $Fc^{+/0}$ (black trace).

Table 3. Summary of electrocatalytic formate oxidation data.

catalyst	k_{obs} (h^{-1})[a]	j (mA/cm^2)[b]	FE_{CO2} (%)[b]	TON[c]	η_{CO2} (V)[d]
1	< 4	-0.24 ± 0.03	99 ± 3	3.9 ± 0.9	0.45
2	135 ± 8	-0.09 ± 0.03	96 ± 3	10.7 ± 2.3	0.57
none	n/a	< 0.001	n/a	n/a	n/a

[a]Average value from four CA trials. [b]Average value from three CPE trials over 95 minutes. [c]Calculated from the ratio of moles of CO_2 produced and total moles of catalyst. [d]Calculated from the difference in $E_{1/2}(Co^{III}\text{-formate}/Co^{II}\text{-formate})$ and $E^0(CO_2/HCOO^-)$.

The CA and CPE studies both indicate that **2** is the most active electrocatalyst in this series. We also probed the stability of **2** under the electrolysis conditions over longer timescales (Figure S68). The current density for formate oxidation is initially stable and then gradually decreases as the reaction proceeds. After 4.3 h, while maintaining the applied potential at the working electrode, the solution was spiked with more formate (50 eq), resulting in an immediate increase in current

density to ca. 70% of the starting value. The behavior indicates that the majority of the catalyst is still active at this point, and the current decay is largely due to substrate consumption. After 10 h, the electrolysis was stopped, and CV analysis of the solution revealed ca. 40% of the PNP complex remains intact. Thus, while clearly some decomposition of **2** occurs during operation, the catalyst structure maintains reasonable integrity and activity over several hours.

The overpotential for formate oxidation is estimated to be 0.45 and 0.57 V for **1** and **2**, respectively, based on the difference between the catalytic half-current potential (taken to be $E_{1/2}$(Co^{III}-formate/Co^{II}-formate)) and the standard thermodynamic potential for this reaction (E^o = -1.40 V vs. $Fc^{+/0}$).[22, 55] Overall, these data unambiguously establish **1** and **2** as competent electrocatalysts for formate oxidation. This series marks the fourth example of a molecular electrocatalyst for this reaction and only the second catalyst family based on a first-row transition metal. Both **1** and **2** are highly selective for CO_2 production, operate at modest overpotentials at 25 °C, and do not require additional exogeneous base to promote turnover. The overpotentials for **1** and **2** are comparable to the values reported for the Ni-P_2N_2 catalysts (η = 0.42 – 0.78 V).[56] The iridium catalyst reported by Kang and co-workers operates at a significantly larger overpotential (η = 1.25 V), though the catalytic rates of the nickel and iridium systems are faster than our cobalt catalysts.[36] Finally, we highlight that **1** and **2** are the first homogeneous cobalt-based electrocatalysts for formate oxidation. Cobalt catalysts for the chemical dehydrogenation of formic acid are also exceedingly rare, and both examples require elevated temperatures for turnover.[57-58]

The observed reactivity of complexes **1**-**3** with formate depends on the reaction conditions. Initial formation of the Co^{III}-formate adduct is followed by hydride transfer to generate the Co^{III}-hydride with the concomitant release of CO_2 (Scheme 3). Deprotonation of the Co^{III}-hydride by formate generates the Co^{I} complex, which, in the absence of applied potential, undergoes rapid comproportionation with Co^{III}-X under stoichiometric conditions (X = MeCN or formate). At higher concentrations of formate, the buffering capacity of the biformate salt maintains sufficient solution basicity and the complex remains in the Co^{I} form. Under electrochemical conditions at an appropriate applied potential, electrocatalytic turnover for formate oxidation is accessible via oxidation of the Co^{I} species at the electrode, regenerating the Co^{III}-formate and closing the electrocatalytic cycle (Scheme 4). In this proposal, hydride transfer is reasonably assigned as the rate-limiting step. The greater catalytic activity of the PNP system **2** compared to the P_2N_2 complex **1** may suggest that the rate of hydride transfer is largely driven by the hydride affinity of the

catalyst and may not directly involve the pendent amine base, though a larger dataset of catalyst structures is needed to establish meaningful trends. Further studies to investigate the precise mechanism of hydride transfer and possible ligand involvement are currently underway.

Scheme 4. Proposed mechanism for electrocatalytic formate oxidation with **1** and **2**. S = acetonitrile. S = acetonitrile.

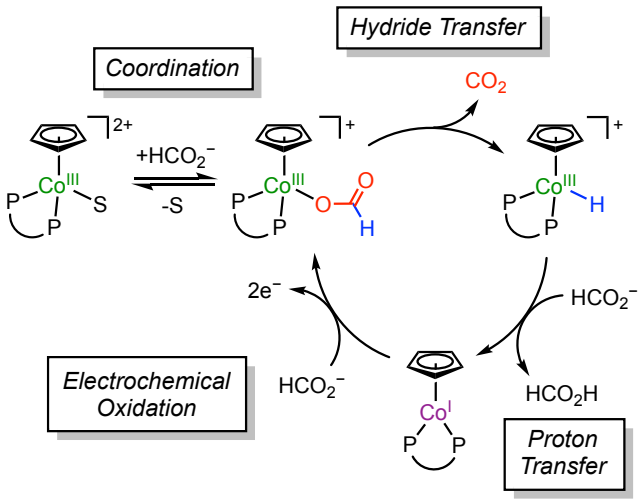

Conclusions

Homogeneous examples of electrocatalysts for formate oxidation are extremely limited, and only one previous report has disclosed this activity at first-row transition metal systems. Herein, we have described a family of piano-stool cobalt complexes based on bidentate phosphine ligands that promote electrocatalytic formate oxidation. We have isolated three classes of complexes in this family in which the structure of the phosphine backbone was varied, and in each case the $[Co^{III}\text{-MeCN}]^{2+}$, $[Co^{I}]^{0}$, and $[Co^{III}\text{-hydride}]^{+}$ complexes were prepared. Detailed characterization of these complexes was performed to obtain key thermodynamic metrics. Importantly, the determination of the thermodynamic hydricity of each Co^{III}-hydride indicated that hydride transfer from the formate anion to the Co^{III} center should be highly favorable in acetonitrile, which was confirmed through chemical reactivity studies. In addition, the acidity of the Co^{III}-hydride complexes is such that formate can serve as a base to facilitate deprotonation, eliminating the need for stronger exogeneous base. While the dppp complex **3** exhibited limited stability in the presence of formate in solution, the P_2N_2 and PNP complexes **1** and **2** are active

electrocatalysts, selectively affording CO_2 with excellent faradaic efficiency. Complex **2** delivered the highest activity for formate oxidation, with the observed rate constant determined by CA being 135 h^{-1}. This complex also exhibited reasonable stability over several hours of operation. This study represents the first cobalt-based and fourth overall example of homogeneous electrocatalysts for formate oxidation. Future work will focus on understanding the hydride transfer mechanism in detail and developing new catalyst structures to increase the rate of this process.

ASSOCIATED CONTENT

Supporting Information

The following files are available free of charge.

- Experimental procedures, crystallographic details, additional data, computational methods, and Cartesian coordinates for DFT calculated structures (PDF)

Accession Codes

CDCC 2227113-2227114, 2231484-2231487, and 2286870-2286872 contains the supplemental crystallographic data for this paper. These data can be obtained free of charge via www.ccdc.cam.ac.uk/data_request/cif, or by emailing data_request@ccdc.cam.ac.uk, or by contacting The Cambridge Crystallographic Data Centre, 12 Union Road, Cambridge CB2 1EZ, UK; fax: +44 1223 336033.

AUTHOR INFORMATION

Corresponding Author

Kate M. Waldie – Department of Chemistry and Chemical Biology, Rutgers, The State University of New Jersey, New Brunswick, New Jersey 08903, United States; orcid.org/0000-0001-6444-6122; Email: kate.waldie@rutgers.edu

Authors

Sriram Katipamula - Department of Chemistry and Chemical Biology, Rutgers, The State University of New Jersey, New Brunswick, New Jersey 08903, United States; orcid.org/0000-0003-2462-5964

Andrew W. Cook - Department of Chemistry and Chemical Biology, Rutgers, The State University of New Jersey, New Brunswick, New Jersey 08903, United States; Present Address: College of Mount Saint Vincent, Riverdale, New York 10471, United States; orcid.org/0000-0002-8850-8946

Isabella Niedzwiecki - Department of Chemistry and Chemical Biology, Rutgers, The State University of New Jersey, New Brunswick, New Jersey 08903, United States; Present Address: Department of Chemistry, Johns Hopkins University, Baltimore, Maryland 21218, United States

Thomas J. Emge - Department of Chemistry and Chemical Biology, Rutgers, The State University of New Jersey, New Brunswick, New Jersey 08903, United States

Author Contributions

Conceptualization, S.K., A.W.C., and K.M.W.; methodology, S.K., A.W.C., and K.M.W.; investigation, S.K., A.W.C., I.N., and T.J.E.; writing – original draft, S.K. and K.M.W.; writing – review and editing; S.K. and K.M.W.; supervision, K.M.W.

Notes

The authors declare no competing financial interests.

ACKNOWLEDGMENTS

This work was supported by Rutgers, The State University of New Jersey. The Rigaku SYNERGY-S X-ray diffractometer was partially funded by an NSF MRI Award (CHE-2117792) to the Rutgers University Department of Chemistry and Chemical Biology.

REFERENCES

1. Lubitz, W.; Tumas, W., Hydrogen: An Overview. *Chem. Rev.* **2007,** *107* (10), 3900-3903. DOI: 10.1021/cr050200z.

2. Oliveira, A. M.; Beswick, R. R.; Yan, Y., A green hydrogen economy for a renewable energy society. *Curr. Opin. Chem. Eng.* **2021,** *33*, 100701. DOI: 10.1016/j.coche.2021.100701.

3. Abe, J. O.; Popoola, A. P. I.; Ajenifuja, E.; Popoola, O. M., Hydrogen energy, economy and storage: Review and recommendation. *Int. J. Hydrogen Energy* **2019,** *44* (29), 15072-15086. DOI: 10.1016/j.ijhydene.2019.04.068.

4. *The Future of Hydrogen*; International Energy Agency, 2019.

5. Preuster, P.; Papp, C.; Wasserscheid, P., Liquid Organic Hydrogen Carriers (LOHCs): Toward a Hydrogen-free Hydrogen Economy. *Acc. Chem. Res.* **2017,** *50* (1), 74-85. DOI: 10.1021/acs.accounts.6b00474.

6. Eppinger, J.; Huang, K.-W., Formic Acid as a Hydrogen Energy Carrier. *ACS Energy Lett.* **2017,** *2* (1), 188-195. DOI: 10.1021/acsenergylett.6b00574.

7. Li, Z.; Xu, Q., Metal-Nanoparticle-Catalyzed Hydrogen Generation from Formic Acid. *Acc. Chem. Res.* **2017,** *50* (6), 1449-1458. DOI: 10.1021/acs.accounts.7b00132.

8. An, L.; Chen, R., Direct formate fuel cells: A review. *J. Power Sources* **2016,** *320*, 127-139. DOI: 10.1016/j.powsour.2016.04.082.

9. Yu, X.; Manthiram, A., Catalyst-selective, scalable membraneless alkaline direct formate fuel cells. *Appl. Catal., B* **2015,** *165*, 63-67. DOI: 10.1016/j.apcatb.2014.09.069.

10. Xiong, Y.; Dong, J.; Huang, Z.-Q.; Xin, P.; Chen, W.; Wang, Y.; Li, Z.; Jin, Z.; Xing, W.; Zhuang, Z.; Ye, J.; Wei, X.; Cao, R.; Gu, L.; Sun, S.; Zhuang, L.; Chen, X.; Yang, H.; Chen, C.; Peng, Q.; Chang, C.-R.; Wang, D.; Li, Y., Single-atom Rh/N-doped carbon electrocatalyst for formic acid oxidation. *Nature Nanotechnol.* **2020,** *15* (5), 390-397. DOI: 10.1038/s41565-020-0665-x.

11. Zhao, Y.; Zhang, K.; Li, Y.; Li, C.; Zhao, R.; Ji, Y.; Meng, Y.; Hu, T.; Wang, H.; Yang, Z.; Yan, Y.-M., Enhanced Electrocatalytic Oxidation of Formate via Introducing Surface Reactive Oxygen Species to a CeO2 Substrate. *ACS Appl. Mater. Interfaces* **2021,** *13* (43), 51643-51651. DOI: 10.1021/acsami.1c12637.

12. Sun, H.-Y.; Ding, Y.; Yue, Y.-Q.; Zue, Q.; Li, F.-M.; Jiang, J.-X.; Chen, P.; Chen, Y., Bifunctional Palladium Hydride Nanodendrite Electrocatalysts for Hydrogen Evolution Integrated with Formate Oxidation. *ACS Appl. Mater. Interfaces* **2021,** *13* (11), 13149-13157. DOI: 10.1021/acsami.0c22106.

13. Guo, L.; Jin, T.; Tang, Q.; Wang, J.; Pan, B.; Wang, Q.; Li, Z.; Wang, C.; Liu, J.; Chen, F., Reconstruction of an AgPd nanoalloy with oxidation for formate oxidation electrocatalysis. *J. Mater. Chem. A* **2022,** *10* (26), 13998-14010. DOI: 10.1039/D2TA01890J.

14. Galan, B. R.; Schöffel, J.; Linehan, J. C.; Seu, C.; Appel, A. M.; Roberts, J. A. S.; Helm, M. L.; Kilgore, U. J.; Yang, J. Y.; DuBois, D. L.; Kubiak, C. P., Electrocatalytic Oxidation of Formate by [Ni(PR2NR′2)2(CH3CN)]2+ Complexes. *J. Am. Chem. Soc.* **2011,** *133* (32), 12767-12779. DOI: 10.1021/ja204489e.

15. Seu, C. S.; Appel, A. M.; Doud, M. D.; DuBois, D. L.; Kubiak, C. P., Formate oxidation via β-deprotonation in [Ni(PR2NR′2)2(CH3CN)]2+ complexes. *Energy Environ. Sci.* **2012,** *5* (4), 6480-6490. DOI: 10.1039/C2EE03341K.

16. Bi, J.; Hou, P.; Kang, P., Single Iridium Pincer Complex for Roundtrip Electrochemical Conversion between Carbon Dioxide and Formate. *ChemCatChem* **2019,** *11* (8), 2069-2072. DOI: 10.1002/cctc.201900083.

17. Cunningham, D. W.; Barlow, J. M.; Velazquez, R. S.; Yang, J. Y., Reversible and Selective CO2 to HCO2− Electrocatalysis near the Thermodynamic Potential. *Angew. Chem. Int. Ed.* **2020,** *59* (11), 4443-4447. DOI: 10.1002/anie.201913198.

18. Xue, L.; Ahlquist, M. S. G., A DFT Study: Why Do [Ni(PR2NR′2)2]2+ Complexes Facilitate the Electrocatalytic Oxidation of Formate? *Inorg. Chem.* **2014,** *53* (7), 3281-3289. DOI: 10.1021/ic4027317.

19. Wiedner, E. S.; Chambers, M. B.; Pitman, C. L.; Bullock, R. M.; Miller, A. J. M.; Appel, A. M., Thermodynamic Hydricity of Transition Metal Hydrides. *Chem. Rev.* **2016,** *116* (15), 8655-8692. DOI: 10.1021/acs.chemrev.6b00168.

20. DuBois, D. L.; Berning, D. E., Hydricity of transition-metal hydrides and its role in CO2 reduction. *Appl. Organomet. Chem.* **2000,** *14* (12), 860-862. DOI: 10.1002/1099-0739(200012)14:12<860::Aid-aoc87>3.0.Co;2-a.

21. Cook, A. W.; Emge, T. J.; Waldie, K. M., Insights into Formate Oxidation by a Series of Cobalt Piano-Stool Complexes Supported by Bis(phosphino)amine Ligands. *Inorg. Chem.* **2021,** *60* (10), 7372-7380. DOI: 10.1021/acs.inorgchem.1c00563.

22. Waldie, K. M.; Ostericher, A. L.; Reineke, M. H.; Sasayama, A. F.; Kubiak, C. P., Hydricity of Transition-Metal Hydrides: Thermodynamic Considerations for CO2 Reduction. *ACS Catal.* **2018,** *8* (2), 1313-1324. DOI: 10.1021/acscatal.7b03396.

23. Fang, M.; Wiedner, E. S.; Dougherty, W. G.; Kassel, W. S.; Liu, T.; DuBois, D. L.; Bullock, R. M., Cobalt Complexes Containing Pendant Amines in the Second Coordination Sphere as Electrocatalysts for H2 Production. *Organometallics* **2014,** *33* (20), 5820-5833. DOI: 10.1021/om5004607.

24. Koelle, U.; Paul, S., Electrochemical reduction of protonated cyclopentadienylcobalt phosphine complexes. *Inorg. Chem.* **1986,** *25* (16), 2689-2694. DOI: 10.1021/ic00236a007.

25. van der Meer, M.; Glais, E.; Siewert, I.; Sarkar, B., Electrocatalytic Dihydrogen Production with a Robust Mesoionic Pyridylcarbene Cobalt Catalyst. *Angew. Chem. Int. Ed.* **2015,** *54* (46), 13792-13795. DOI: 10.1002/anie.201506061.

26. Roy, S.; Sharma, B.; Pécaut, J.; Simon, P.; Fontecave, M.; Tran, P. D.; Derat, E.; Artero, V., Molecular Cobalt Complexes with Pendant Amines for Selective Electrocatalytic Reduction of Carbon Dioxide to Formic Acid. *J. Am. Chem. Soc.* **2017,** *139* (10), 3685-3696. DOI: 10.1021/jacs.6b11474.

27. Curtis, C. J.; Miedaner, A.; Ciancanelli, R.; Ellis, W. W.; Noll, B. C.; Rakowski DuBois, M.; DuBois, D. L., [Ni(Et2PCH2NMeCH2PEt2)2]2+ as a Functional Model for Hydrogenases. *Inorg. Chem.* **2003,** *42* (1), 216-227. DOI: 10.1021/ic020610v.

28. Helm, M. L.; Stewart, M. P.; Bullock, R. M.; DuBois, M. R.; DuBois, D. L., A Synthetic Nickel Electrocatalyst with a Turnover Frequency Above 100,000 s^{−1} for H₂ Production. *Science* **2011,** *333* (6044), 863-866. DOI: 10.1126/science.1205864.

29. Liu, T.; DuBois, D. L.; Bullock, R. M., An iron complex with pendent amines as a molecular electrocatalyst for oxidation of hydrogen. *Nat. Chem.* **2013,** *5* (3), 228-233. DOI: 10.1038/nchem.1571.

30. Yang, J. Y.; Bullock, R. M.; Dougherty, W. G.; Kassel, W. S.; Twamley, B.; DuBois, D. L.; Rakowski DuBois, M., Reduction of oxygen catalyzed by nickel diphosphine complexes with positioned pendant amines. *Dalton Trans.* **2010,** *39* (12), 3001-3010. DOI: 10.1039/B921245K.

31. Weiss, C. J.; Egbert, J. D.; Chen, S.; Helm, M. L.; Bullock, R. M.; Mock, M. T., Protonation Studies of a Tungsten Dinitrogen Complex Supported by a Diphosphine Ligand Containing a Pendant Amine. *Organometallics* **2014,** *33* (9), 2189-2200. DOI: 10.1021/om401127v.

32. Weiss, C. J.; Wiedner, E. S.; Roberts, J. A. S.; Appel, A. M., Nickel phosphine catalysts with pendant amines for electrocatalytic oxidation of alcohols. *Chem. Commun.* **2015,** *51* (28), 6172-6174. DOI: 10.1039/C5CC01107H.

33. Bhattacharya, P.; Heiden, Z. M.; Wiedner, E. S.; Raugei, S.; Piro, N. A.; Kassel, W. S.; Bullock, R. M.; Mock, M. T., Ammonia Oxidation by Abstraction of Three Hydrogen Atoms from a Mo–NH3 Complex. *J. Am. Chem. Soc.* **2017,** *139* (8), 2916-2919. DOI: 10.1021/jacs.7b00002.

34. Wiedner, E. S.; Appel, A. M.; Raugei, S.; Shaw, W. J.; Bullock, R. M., Molecular Catalysts with Diphosphine Ligands Containing Pendant Amines. *Chem. Rev.* **2022,** *122* (14), 12427-12474. DOI: 10.1021/acs.chemrev.1c01001.

35. Galan, B. R.; Reback, M. L.; Jain, A.; Appel, A. M.; Shaw, W. J., Electrocatalytic Oxidation of Formate with Nickel Diphosphine Dipeptide Complexes: Effect of Ligands Modified with Amino Acids. *Eur. J. Inorg. Chem.* **2013,** *2013* (30), 5366-5371. DOI: 10.1002/ejic.201300751.

36. Waldie, K. M.; Katipamula, S., Recent Progress in the Development of Molecular Electrocatalysts for Formate Oxidation. *Catalysis Research* **2022,** *02* (01), 006. DOI: 10.21926/cr.2201006.

37. Weiss, C. J.; Groves, A. N.; Mock, M. T.; Dougherty, W. G.; Kassel, W. S.; Helm, M. L.; DuBois, D. L.; Bullock, R. M., Synthesis and reactivity of molybdenum and tungsten bis(dinitrogen) complexes supported by diphosphine chelates containing pendant amines. *Dalton Trans.* **2012,** *41* (15), 4517-4529. DOI: 10.1039/C2DT12224C.

38. Fraze, K.; Wilson, A. D.; Appel, A. M.; Rakowski DuBois, M.; DuBois, D. L., Thermodynamic Properties of the Ni−H Bond in Complexes of the Type

[HNi(P2RN2R‘)2](BF4) and Evaluation of Factors That Control Catalytic Activity for Hydrogen Oxidation/Production. *Organometallics* **2007,** *26* (16), 3918-3924. DOI: 10.1021/om070143v.

39. Waldie, K. M.; Kim, S.-K.; Ingram, A. J.; Waymouth, R. M., Cyclopentadienyl Cobalt Complexes as Precatalysts for Electrocatalytic Hydrogen Evolution. *Eur. J. Inorg. Chem.* **2017,** *2017* (20), 2755-2761. DOI: 10.1002/ejic.201700188.

40. Kurtz, D. A.; Dhar, D.; Elgrishi, N.; Kandemir, B.; McWilliams, S. F.; Howland, W. C.; Chen, C.-H.; Dempsey, J. L., Redox-Induced Structural Reorganization Dictates Kinetics of Cobalt(III) Hydride Formation via Proton-Coupled Electron Transfer. *J. Am. Chem. Soc.* **2021,** *143* (9), 3393-3406. DOI: 10.1021/jacs.0c11992.

41. Elgrishi, N.; Kurtz, D. A.; Dempsey, J. L., Reaction Parameters Influencing Cobalt Hydride Formation Kinetics: Implications for Benchmarking H2-Evolution Catalysts. *J. Am. Chem. Soc.* **2017,** *139* (1), 239-244. DOI: 10.1021/jacs.6b10148.

42. Berning, D. E.; Noll, B. C.; DuBois, D. L., Relative Hydride, Proton, and Hydrogen Atom Transfer Abilities of [HM(diphosphine)2]PF6 Complexes (M = Pt, Ni). *J. Am. Chem. Soc.* **1999,** *121* (49), 11432-11447. DOI: 10.1021/ja991888y.

43. Brereton, K. R.; Smith, N. E.; Hazari, N.; Miller, A. J. M., Thermodynamic and kinetic hydricity of transition metal hydrides. *Chem. Soc. Rev.* **2020,** *49* (22), 7929-7948. DOI: 10.1039/D0CS00405G.

44. Tshepelevitsh, S.; Kütt, A.; Lõkov, M.; Kaljurand, I.; Saame, J.; Heering, A.; Plieger, P. G.; Vianello, R.; Leito, I., On the Basicity of Organic Bases in Different Media. *Eur. J. Org. Chem.* **2019,** *2019* (40), 6735-6748. DOI: 10.1002/ejoc.201900956.

45. Raebiger, J. W.; Miedaner, A.; Curtis, C. J.; Miller, S. M.; Anderson, O. P.; DuBois, D. L., Using Ligand Bite Angles To Control the Hydricity of Palladium Diphosphine Complexes. *J. Am. Chem. Soc.* **2004,** *126* (17), 5502-5514. DOI: 10.1021/ja0395240.

46. Curtis, C. J.; Miedaner, A.; Raebiger, J. W.; DuBois, D. L., Periodic Trends in Metal Hydride Donor Thermodynamics: Measurement and Comparison of the Hydride Donor Abilities of the Series HM(PNP)2+ (M = Ni, Pd, Pt; PNP = Et2PCH2N(Me)CH2PEt2). *Organometallics* **2004,** *23* (3), 511-516. DOI: 10.1021/om0342816.

47. Stirling, M. J.; Sweeney, G.; MacRory, K.; Blacker, A. J.; Page, M. I., The kinetics and mechanism of the organo-iridium-catalysed enantioselective reduction of imines. *Org. Biomol. Chem.* **2016,** *14* (14), 3614-3622. DOI: 10.1039/C6OB00245E.

48. Bard, A. J.; Faulkner, L. R., *Electrochemical Methods: Fundamentals and Applications*. 2nd ed.; John Wiley & Sons: 2001.

49. Delahay, P.; Stiehl, G. L., Theory of Catalytic Polarographic Currents. *J. Am. Chem. Soc.* **1952,** *74* (14), 3500-3505. DOI: 10.1021/ja01134a014.

50. Artero, V.; Fontecave, M., Solar fuels generation and molecular systems: is it homogeneous or heterogeneous catalysis? *Chem. Soc. Rev.* **2013,** *42* (6), 2338-2356. DOI: 10.1039/C2CS35334B.

51. Cobo, S.; Heidkamp, J.; Jacques, P.-A.; Fize, J.; Fourmond, V.; Guetaz, L.; Jousselme, B.; Ivanova, V.; Dau, H.; Palacin, S.; Fontecave, M.; Artero, V., A Janus cobalt-based catalytic material for electro-splitting of water. *Nat. Mater.* **2012,** *11* (9), 802-807. DOI: 10.1038/nmat3385.

52. Anxolabéhère-Mallart, E.; Costentin, C.; Fournier, M.; Nowak, S.; Robert, M.; Savéant, J.-M., Boron-Capped Tris(glyoximato) Cobalt Clathrochelate as a Precursor for the Electrodeposition of Nanoparticles Catalyzing H2 Evolution in Water. *J. Am. Chem. Soc.* **2012,** *134* (14), 6104-6107. DOI: 10.1021/ja301134e.

53. Kaeffer, N.; Chavarot-Kerlidou, M.; Artero, V., Hydrogen Evolution Catalyzed by Cobalt Diimine–Dioxime Complexes. *Acc. Chem. Res.* **2015,** *48* (5), 1286-1295. DOI: 10.1021/acs.accounts.5b00058.

54. Kaeffer, N.; Morozan, A.; Fize, J.; Martinez, E.; Guetaz, L.; Artero, V., The Dark Side of Molecular Catalysis: Diimine–Dioxime Cobalt Complexes Are Not the Actual Hydrogen Evolution Electrocatalyst in Acidic Aqueous Solutions. *ACS Catal.* **2016,** *6* (6), 3727-3737. DOI: 10.1021/acscatal.6b00378.

55. Appel, A. M.; Helm, M. L., Determining the overpotential for a molecular electrocatalyst. *ACS Catal.* **2014,** *4* (2), 630-633. DOI: 10.1021/cs401013v.

56. Waldie, K. M.; Brunner, F. M.; Kubiak, C. P., Transition Metal Hydride Catalysts for Sustainable Interconversion of CO2 and Formate: Thermodynamic and Mechanistic Considerations. *ACS Sustainable Chem. Eng.* **2018,** *6* (5), 6841-6848. DOI: 10.1021/acssuschemeng.8b00628.

57. Zhou, W.; Wei, Z.; Spannenberg, A.; Jiao, H.; Junge, K.; Junge, H.; Beller, M., Cobalt-Catalyzed Aqueous Dehydrogenation of Formic Acid. *Chem. Eur. J.* **2019,** *25*, 8459-8464. DOI: 10.1002/chem.201805612.

58. Lentz, N.; Aloisi, A.; Thuéry, P.; Nicolas, E.; Cantat, T., Additive-Free Formic Acid Dehydrogenation Catalyzed by a Cobalt Complex. *Organometallics* **2021,** *40* (5), 565-569. DOI: 10.1021/acs.organomet.0c00777.